A novel method for the design of proximity sensor configuration for rotor blade tip timing

David H. Diamond

Postdoctoral Fellow
Centre for Asset Integrity Management
Department of Mechanical and Aeronautical Engineering
University of Pretoria
Pretoria 0002, South Africa
Email: dawie.diamond@up.ac.za

P. Stephan Heyns

Director
Centre for Asset Integrity Management
Department of Mechanical and Aeronautical Engineering
University of Pretoria
Pretoria 0002, South Africa
Email: stephan.heyns@up.ac.za

Blade Tip Timing is a non-contact method for the measurement of turbomachinery blade vibration. Proximity sensors are mounted circumferentially around the turbomachine casing and used to measure the tip displacement of blades during operation. The processing of these tip deflections is, however, riddled with complications such as aliasing, high levels of noise and non-equidistant samples in the time domain. Specialized BTT algorithms have been developed to extract as much information as possible from the signals. The utility of these algorithms depend on the circumferential spacing between the proximity sensors. If the spacing is sub-optimal, an algorithm can fail to measure dangerous blade vibration. This article presents a novel method to determine the spacing between the proximity sensors such that the Blade Tip Timing system can be used to measure blade vibration as accurately as possible.

1   Introduction

Blade Tip Timing (BTT) is a non-contact method for measuring turbomachinery blade vibration during operation [1–4]. BTT is an alternative to strain gauge systems. Strain gauge systems are considered the conventional technique for measuring rotor blade dynamics [3]. Strain gauge technology, however, has several drawbacks, such as high cost of installation, limited lifetime due to harsh operating conditions, and the fact that it can only be installed on a small number of blades [3, 5]. Faster turbomachine development cycles and high strain gauge system mortality rates, among other reasons, have led to decreased use of strain gauges

in favor of a combination of BTT and Finite Element (FE) models [6]. BTT uses proximity sensors mounted circum-
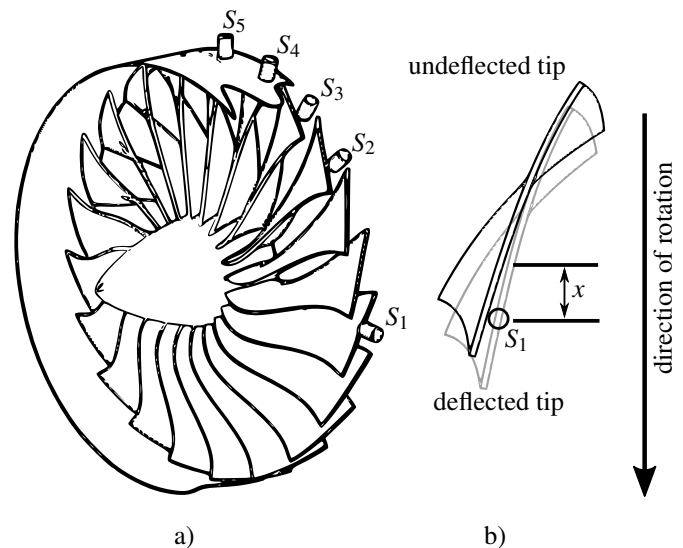

Fig. 1: Principle behind BTT. a) A compressor fan row with a broken out casing is shown with five proximity sensors (numbered S_1 through S_5) above the row, b) the deflected blade tip arrives earlier than the undeflected tip due to the tip deflection.

ferentially around a turbomachine rotor stage into the casing (Fig. 1 a). The Time of Arrival (ToA) of each blade as it

1

passes underneath each sensor is then measured. A blade that is not experiencing any vibration will have an expected ToA based on the known shaft rotation speed. A vibrating blade will arrive earlier or later than expected due to its tip deflection, x (Fig. 1 b). The difference between these two ToAs, Δt, is used to calculate the rotor blade tip displacement, usually with Eq. 1

$$x = \Delta t \Omega R \qquad (1)$$

where R is the rotor's outside radius and Ω is the rotor rotational speed. Each time a rotor blade passes underneath a sensor, the BTT system obtains one measurement. By taking measurements from several sensors and multiple shaft rotations, one can attempt to infer the blade vibration amplitude and frequency.

The inference of rotor blade vibration is, however, notoriously difficult to perform, especially if the vibration is an integer multiple, or Engine Order (EO) of the shaft speed [7, 8]. The frequency of EO excited vibration is calculated with Eq. 2

$$f = EO\Omega \qquad (2)$$

where f is the excitation frequency in Hertz. The difficulty in measuring EO vibration is because the BTT system measures the same part of the blade's vibration cycle each time it passes a particular sensor. As such, no substantial information is added by measuring for more than one shaft revolution.

Another factor that contributes to the difficulty of processing BTT signals is aliasing [9, 10]. In most other measurement activities, aliasing is caused by a limited data acquisition sampling rate. In BTT however, the sampling rate is completely determined by the rotational speed of the rotor and the number and spacing of the sensors in the rotor casing. Consider, for instance, a rotor turning at a speed of 50 Hz that is surrounded by 8 proximity sensors. The sensors are installed equidistant from one another around the casing. This leads to a sampling rate of 400 Hz for each blade (8 measurements taken 50 times per second) and a Nyquist frequency of 200 Hz. Rotor blades often have natural frequencies above 200 Hz, which would make these signals difficult to process using conventional signal processing techniques. BTT signals are, in addition to this, extremely noisy and contain latent signals from shaft torsional vibration and casing vibration. Specialized BTT signal processing techniques have therefore been developed to extract as much meaningful information from the signals as possible [1–4, 7–9, 11–21].

All of these methods require tip displacement measurements of the highest possible quality to maximize the accuracy of the inference. One aspect that greatly influences a BTT system's signal quality is the sensor circumferential configuration. Poorly or inadequately spaced sensors can lead to signals that are more sensitive to noise and which contain less information. The machining of sensor mounting holes is financially expensive and the resulting sensor configuration is permanent. An incorrectly designed sensor configuration can therefore lead to a BTT system that does not deliver on its intended goal, or does not deliver at all. Some methods require sensors spaced in an equidistant manner [1,19] and other methods can use any type of sensor spacing.

This article presents a novel method to determine the non-equidistant sensor configuration that will maximize the information in the signals measured by a BTT system. An approach used by some in industry [22] is described and developed further into a constrained optimization problem. An example sensor configuration design is performed on a rotor with realistic natural frequencies and operational conditions, thereby illustrating the method.

2 Sensor positioning

Consider three different BTT systems, identical in the number of sensors but each with a different sensor configuration. Each BTT system has 5 sensors with a configuration shown in Tab. 1. The BTT systems are installed onto the

Table 1: Sensor positions for the three different BTT systems. Angles in radians.

BTT System	θ_1	θ_2	θ_3	θ_4	θ_5
1	0.35	1.40	2.44	3.49	4.54
2	0.45	1.81	2.54	3.91	4.64
3	0.55	1.55	3.15	4.45	4.75

same rotor. The rotor has a first natural frequency of 300 Hz and is rotating at a rate of 50 Hz. The first natural frequency is excited by an EO 6 disturbance, caused by obstructions in the working fluid flow path [23,24]. The vibration amplitude is 200 μm. The measurements taken by each BTT system is shown in Fig. 2. Figure 2 illustrates the varying quality of tip deflection measurements one can obtain from BTT systems with an identical amounts of sensors but different configurations. All the sensors in BTT system 1 measure the blade vibration at exactly the same location in the rotor blade's vibration cycle. The value of 50 μm is measured repeatedly. It would be impossible for an algorithm to calculate the natural frequency from what is essentially a DC offset signal. This arrangement is sub-optimal and should be avoided.

BTT system 2 measures two different tip displacements, -67 μm and -158.3 μm. Although some variability among the measurements are present, only one direction of vibration is measured (negative direction). This would also make accurate inference difficult if not impossible.

BTT system 3 measures unique parts of the vibration signal which span to both directions of motion. An algorithm has a much better chance of inferring the true natural frequency and vibration amplitude from this signal as all its
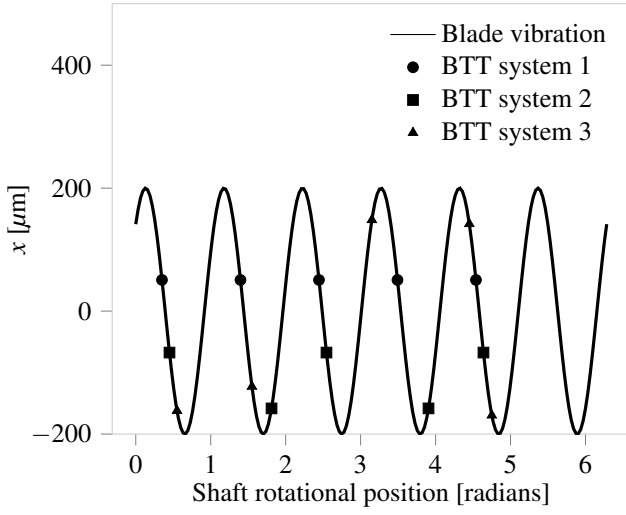
Fig. 2: Different measurements taken by three different sensor arrangements for an EO 6 vibration of size 200 μm.

values are unique. This arrangement should always be preferred above the other two.

There is a mathematical approach to evaluate the quality of BTT sensor configuration. One can express the vibration signal as an orthogonal sinusoid, as done in Eq.3 below,

$$x_i(t) = A\sin(EO\theta_i) + B\cos(EO\theta_i) + C \qquad (3)$$

where A, B and C are the vibration coefficients and θ_i is the circumferential position of the ith sensor. A five sensor BTT system will have five such equations and can be assembled into a system of the form given in Eq. 4

$$\mathbf{\Phi a = b} \qquad (4)$$

where Φ is called the design matrix and is given by Eq. 5.

$$\Phi = \begin{pmatrix} \sin(EO\theta_1) & \cos(EO\theta_1) & 1 \\ \sin(EO\theta_2) & \cos(EO\theta_2) & 1 \\ \sin(EO\theta_3) & \cos(EO\theta_3) & 1 \\ \sin(EO\theta_4) & \cos(EO\theta_4) & 1 \\ \sin(EO\theta_5) & \cos(EO\theta_5) & 1 \end{pmatrix} \qquad (5)$$

The condition number, κ, of the design matrix Φ is a measure of how sensitive the solution to Eq.4 is to permutations in the input values and round off errors during the computing process [25]. A condition number of 1, the minimum possible number, indicates it is possible to recover the vector $\mathbf{a}$ perfectly. A condition number tending to infinity indicates the design matrix is singular and cannot be used to solve the equation. The condition numbers for the three BTT sensors in Tab.1 are reported below in Tab. 2.

In Tab. 2, $\boldsymbol{\theta}$ is the shorthand notation for the set of all sensors. The condition numbers listed in Tab. 2 corroborates the earlier qualitative assessment of the sensor configurations

Table 2: Condition numbers for the design matrices of three different BTT systems.

BTT System	$\kappa(\boldsymbol{\theta}, EO = 6)$
1	3.64×10^{16}
2	2.61×10^{15}
3	2.95

for the different BTT systems. It is seen that BTT system 3 has the lowest condition number by far, meaning it is more likely to recover the true solution in the inevitable case of noise being present in the tip deflection measurements.

The design matrix condition number is therefore a metric that can be minimized to obtain a useful BTT sensor configuration.

3 Optimization problem

When faced with a new BTT installation, the sensor configuration can be designed by formulating and solving an optimization problem. The three main steps in formulating the problem are presented below.

3.1 Establish the number of sensors to be used

A general rule of thumb is that the maximum number of sensors should be preferred. There are, however, limitations to the number of sensors one can use. Sensors that operate long periods of time in harsh conditions tend to be expensive. The cost of a data acquisition system also scales with the number of sensors. Furthermore, there may be limited space for the sensors on the turbomachine. The number of sensors should be chosen as the maximum allowable amount subject to the constraints described above. The number of sensors determine the number of rows in the design matrix.

3.2 Find the EOs of interest

In the previous example of design matrix condition number calculation, an EO=6 has been used for the calculation. It is unlikely that the BTT system will be used to measure blade vibration caused by only one possible EO excitation. A large number of EOs can be included into the optimization problem, say for EOs 1 through 1000. This can however result in a BTT system optimized to measure vibration modes that are not damaging (such as highly damped high-frequency modes) or modes that are unlikely to be excited at all.

Practically, one can limit the EOs being taken into account. For instance, suppose an aircraft engine operates between 3000 RPM (50 Hz) and 6000 RPM (100 Hz) for the majority of its life. The first four natural frequencies of the compressor row being monitored have values of 200, 300, 400 and 500 Hz. If one is only interested in measuring the

first four natural frequencies, one can calculate the minimum EO to be measured by dividing the smallest natural frequency of interest with the largest operational speed, as done in Eq. 6.

$$EO_{\min} = \frac{200}{100} = 2 \qquad (6)$$

The maximum natural frequency of interest can be obtained by dividing the largest natural frequency with the lowest operational speed, as done in Eq. 7.

$$EO_{\max} = \frac{500}{50} = 10 \qquad (7)$$

All EOs between $EO_{\min}$ and $EO_{\max}$ may be excited and the sensors must be optimized to measure all EOs as accurately as possible.

In addition to optimizing for all the EOs in this range, some EOs might be of particular interest. There are many reasons that an EO might be of particular interest. Possible reasons are given below:

1. Turbomachines are often operated at set points, or constant shaft speeds, for extended periods of time. A certain EO excitation at a set point may coincide or near-coincide with a natural frequency of the machine. Take the example of an aircraft with a shaft speed of 4000 RPM for one of its prevalent cruising speeds. If the lowest natural frequency of the first compressor row blades is approximately 540 Hz, this is fairly close to the 8th order excitation at 4000 RPM of 533.3 Hz. This natural frequency might shift downwards to the excitation frequency because of temperature effects or changes in boundary conditions at the root attachment.
2. One may know, from simulations or previous experience, that some modes are more damaging than others and that some EO excitations, such as the lower ones, cause more damage than high EO excitation.
3. One may be aware of a particular failure mode that suggests a specific mode of vibration in a narrow shaft speed range.

A weight factor, w_{EO}, can then be assigned to specific EOs of interest during optimization to place particular emphasis on being able to measure those EOs. The size of the weight must be chosen based on engineering intuition, at least until further research is conducted.

3.3 Find the smallest sum of squared weighted condition numbers

The optimal sensor spacing is now defined as the sensor spacing leading to the minimum sum of squared weighted condition numbers. This is expressed in Eq. 8.

$$\theta_{\mathrm{opt}} = \mathrm{argmin}_{\theta} \left(\sum_{EO=EO_{\min}}^{EO_{\max}} (w_{EO}\kappa(\theta,EO))^2 \right) \qquad (8)$$

Most of the weights will be one, except for those that have been identified as particularly important to measure.

3.4 Particle Swarm Optimization

This optimization problem does not have a single local solution. Consider the case of a three sensor BTT system being analyzed to determine the sensor configuration. All EOs between 2 and 10 are of equal importance and the first sensor is fixed at 0 radians. A heat map of the minimization surface for the remaining two sensors is shown in Fig. 3. In Figure
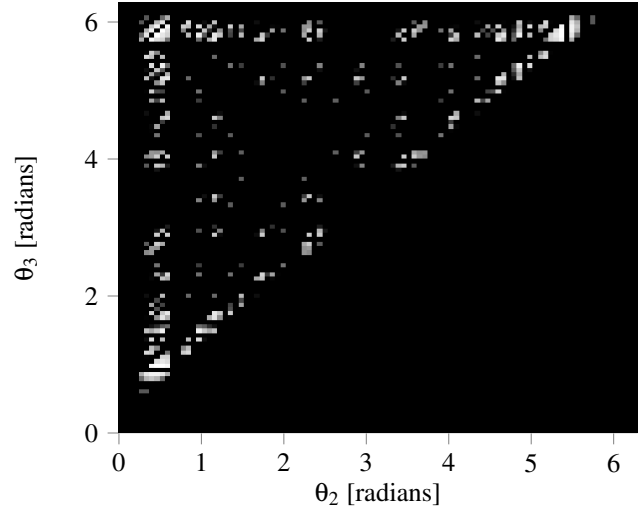

Fig. 3: The error function as a heat map for a three sensor BTT optimization where θ_1 is fixed to 0 radians and the EOs between 2 and 10 are taken into account. Lighter shades indicate better solutions. The sensor spacings are constrained to be monotonically increasing.

3, lighter shades indicate better sensor configurations. It is seen that there are many local minima and a large amount of local maxima. It is therefore a global optimization problem.

Particle Swarm Optimization (PSO) is a well known optimization technique that can be used to solve global optimization problems. PSO is the preferred optimization technique used in this article but could be exchanged with other global optimization techniques.

To determine N sensor positions, the parameter being optimized is θ as shown in Eq. 9 below

$$\theta = (\theta_1, \delta\theta_2, \delta\theta_3, \ldots, \delta\theta_N) \qquad (9)$$

where θ_1 is the absolute circumferential position of the first sensor and Eq. 10 can be used to determine the absolute circumferential positions of the other sensors.

$$\theta_n = \theta_{n-1} + \delta\theta_n \qquad (10)$$

This form of parameter vector ensures that all sensor angles are monotonically increasing in their value. All values of θ

4

are limited to the range $0 - 0.5\pi$. The maximum distance between two subsequent sensors is therefore 0.5π. It has been found that this value leads to the most rapid convergence and best possible solutions for the PSO algorithm. For all runs conducted in this article, a particle swarm size of 5000 was chosen and the optimization ran for 30 iterations.

4 Constraints

There are limitations to the positioning of sensors that must be taken into account. Two types of constraints are taken into account below.

4.1 Minimum sensor distance

Sensors are typically mounted by machining tapped holes into the turbomachine casing. The sensor center distances therefore need to be a certain minimum distance apart. A rule of thumb is that the sensor center distances need to be at least 1.5 hole diameters apart. Additionally, some sensors such as eddy current sensors need to be spaced a minimum distance apart so that the sensors do not interfere with one another. For eddy current sensors, a minimum of three sensor head diameters are usually recommended. One can formulate the constraint between any two sensors i and j as done in Eq. 11.

$$|\Delta\theta_{i,j}| = |\theta_j - \theta_i| \geq \frac{d_{\min}}{R} \tag{11}$$

where $d_{\min}$ is the minimum length on the arc of the casing that must separate sensors. Note that the angles here are mapped into the 0 - 2π range if some are larger than 2π.

4.2 Casing fixtures

Turbomachines are intricate structures with many fixtures and components on the casing. It may not be possible to install sensors on the entire casing circumference. One should therefore create circumferential areas are is unavailable to place the sensors at. Mathematically, this is given by Eq. 12.

$$\theta_i \notin [\theta_{1,\min}^*, \theta_{1,\max}^*] \cup [\theta_{2,\min}^*, \theta_{2,\max}^*] \ldots \cup [\theta_{M,\min}^*, \theta_{M,\max}^*] \tag{12}$$

In Equation 12, $\theta_{m,\min}^*$ and $\theta_{m,\max}^*$ indicate the minimum and maximum fixture locations for the mth fixture.

4.3 Implementing constraints

The implementation of the PSO algorithm used [26] allows for the specification of constraint functions. These functions return a positive value if the solution is valid and a negative function if not.

5 Illustrative example

The proposed method is now illustrated with an example. BTT sensor configuration for a rotor is determined with two different sets of EO weights.

5.1 Rotor row

Consider the characteristics of a compressor blade row in an aircraft engine. The blades have an outside diameter of 440 mm. The natural frequencies of the rotor blades increase with increased operational speed. The rotor blade's first 5 natural frequencies are given in Tab. 3 for rotor speeds at 6800 RPM, 14500 RPM and 15600 RPM. These frequencies correspond to the frequencies presented in [27] for an SO-3 engine. The natural frequencies increase as the speed increases. Suppose further that this engine will operate between 6800 RPM and 15600 RPM for the majority of its operating hours, and that a BTT system should be installed to measure the vibrations during this operating range.

Table 3: Natural frequencies for rotor blades at different shaft speeds. Frequencies in Hertz.

Mode number	6800 RPM	14500 RPM	15600 RPM
1	374.1	489.5	509.2
2	1350.2	1500.5	1527.7
3	1826.4	1856.2	1863.1
4	3058.8	3117.3	3127.8
5	3871.0	4021.0	4051.2

Six microwave sensors are used with a probe diameter of 14mm. The diameter corresponds to the sensor described in [28]. These sensors are fixed into the casing and must be placed 1.5 times the diameter, or 21mm, apart. This leads to a minimum distance between sensors as calculated in Eq.13.

$$\frac{d_{\min}}{R} = \frac{21}{400} = 0.0525 \text{ radians} \tag{13}$$

The compressor has permanent fixtures around the row to be monitored. The permanent fixtures are such that no sensors can be placed at the circumferential locations given in Tab. 4.

Table 4: Minimum and maximum locations of the permanent fixtures around the compressor casing. Values in degrees.

Fixture number	$\theta_{\min}^*$	$\theta_{\max}^*$
1	0	80
2	123	130
3	256	330

5.2 Possible EOs to be excited

The natural frequencies of the rotor blades increase as a function of speed. To be conservative, the minimum and maximum natural frequencies are calculated using the overall minimum and maximum frequencies and the overall minimum and maximum speeds, i.e.

$$EO_{max} = \frac{4051.2}{6800/60} = 35.7 \approx 35 \tag{14}$$

$$EO_{min} = \frac{374.1}{15600/60} = 1.4 \approx 2 \tag{15}$$

When calculating the maximum and minimum EOs and ending with a fraction, the maximum EO is always rounded down to the nearest integer and the minimum EO is always rounded up. All the EO weights of the system are taken as 1, meaning no EO is deemed more important to measure than any other.

The PSO algorithm is now used along with the constraints mentioned in Sec. 4 and Sec. 5.1. As can be seen from Fig. 3, there are many local solutions. Finding a global minimum might be an elusive task for problems with many different EOs and many constraints, such as in this example. To demonstrate this point, four PSO optimization runs are performed and the best solution objective function value for each iteration is shown in Fig. 4. It is seen that all of
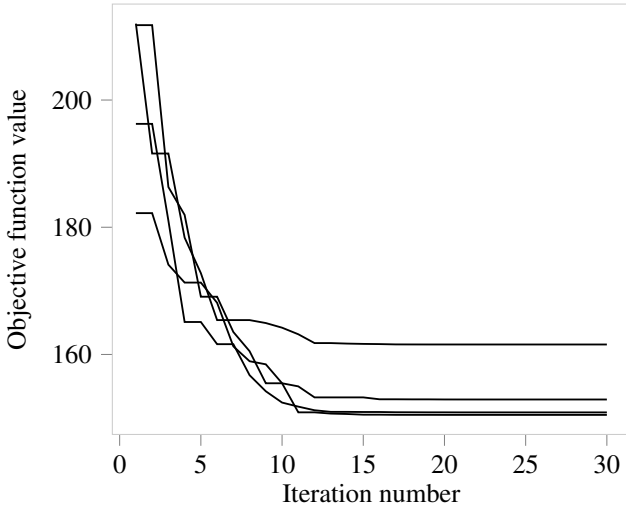

Fig. 4: Progress of PSO algorithm for 4 different runs for the same problem.

the runs start out with an objective function value of between 180 and 220 and decrease gradually to a value of between 150 and 165. Because of the random nature of the PSO algorithm and the multitude of global minima, one should not expect to obtain the same sensor spacing repeatedly. All the solutions are, however, good choices for the sensor spacing. It is advisable to perform many different optimization runs and compare different solutions. The values of the parameter vector for each run is shown in Tab. 5.

It is seen that the first sensor for all four runs are located between 1.72 and 1.90 radians. All sensor increments are between 0.1 and 1.2 radians. Recall the limits of the sensor increments are 0 to 1.57 (or 0.5π) radians. It is seen that no increment reaches 1.57, which suggests that the maximum increment limit is reasonable.

It is also possible to visualize the condition numbers resulting from the use of an optimal solution. This reveals inherent characteristics of the BTT system and can be used to sensitize the designer of some EOs that might be more difficult to pick up than the rest. Figure 5 shows the condition numbers for EOs 2 to 35 for Run 1, the run with the best optimization result. It can be seen from Fig. 5 that condition
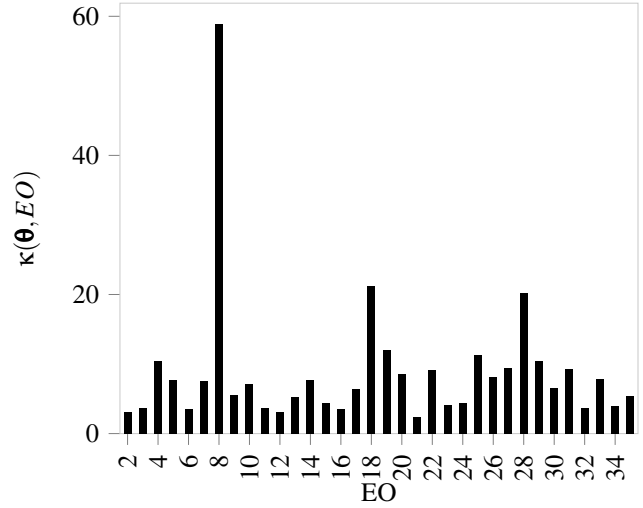

Fig. 5: Condition numbers for different EOs for the Run 1 optimal result.

number values are fairly constant, though a general slight increase in condition number can be seen towards the higher EO values. It can also be seen that the condition number for EO=8 is significantly higher than for any other EO. This indicates that the BTT system installed according to this sensor spacing might have more difficulty to measure EO 8 vibrations that any other vibration.

5.3 Weighted EOs

Suppose it has been decided, through an investigation of the vibration characteristics of the rotor in question, that blade vibrations below EO=9 are more threatening and dangerous than larger vibrations. These EOs can enjoy more importance in the optimization routine by setting the condition number weights, w_{EO}, of all EO values lower than 9 to a higher value than 1. The weights for EOs 2 through 8 are here set to 10 while the other weights are kept at 1.

If the PSO algorithm is repeated with this set of weights, the optimal position is given below in Eq. 16 and the condi-

Table 5: Parameter vector and objective function optimal values for each PSO run.

Run number	θ_1	$\delta\theta_2$	$\delta\theta_3$	$\delta\theta_4$	$\delta\theta_5$	$\delta\theta_6$	Objective function value
1	1.90	0.69	0.16	0.14	0.33	0.41	150.50
2	1.80	1.19	0.54	0.16	0.14	0.32	161.57
3	1.72	0.17	0.15	0.34	0.50	0.88	152.92
4	1.79	1.03	0.15	0.14	0.33	0.40	150.89

tion numbers for all EOs are shown in Fig. 6.

$$\boldsymbol{\theta} = (1.42, 0.32, 0.35, 0.63, 0.65, 0.52) \quad (16)$$

It is seen from Eq. 16 that the first sensor value has a smaller
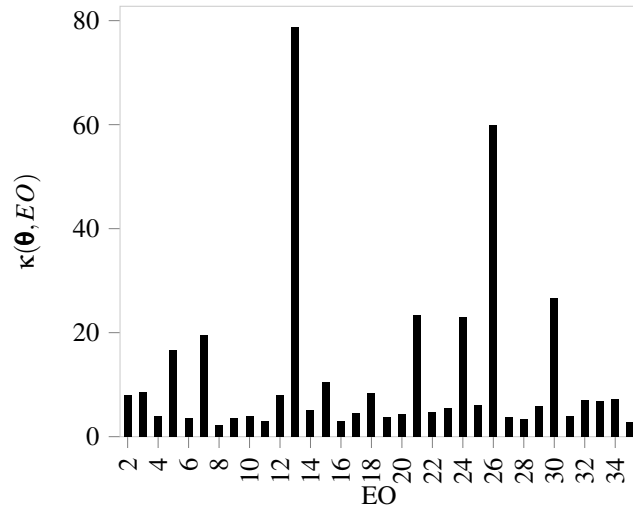

Fig. 6: Condition numbers for different EOs when weighting the EO values lower than 8 more then the remaining EO values.

value, 1.42, than the other optimization results' values. Figure 6 shows that the condition numbers for EOs between 2 and 8 are generally low and do not contain any extreme outliers. Altering the weights of the condition numbers does not guarantee the ability to measure those EOs more accurately but increases the likelihood. If many PSO optimization runs are performed one ends up with a couple of sensor configurations that meet the requirements of the system.

6 Future Research and Limitations

The method presented in this article takes account of only one row of sensors. It is possible that multiple sensor rows will require an amended version of this method and/or may have different constraints. Also, multimode vibration,

where more than one natural frequency is excited simultaneously for each blade, will require an amended version of design matrix construction and should be developed where multimodal vibration is expected. The method proposed in this article should, by definition, not be used where algorithms that require equidistant sensor spacing are going to be used. This method can however be expanded to accommodate equidistant sensor spacing.

7 Conclusion

This article presents a novel method that can be used to calculate the circumferential positions of BTT sensors that allows one to measure several blade vibration frequencies at different EO excitations. The method uses the sum of weighted design matrix condition numbers as a function that must be minimized subject to constraints that may be present in a BTT system installation. It is shown that the optimization problem requires a global optimization algorithm as the problem does not lend itself to local solutions. The method is demonstrated using an example rotor.

References

[1] Zielinski, M., and Ziller, G., 2000. "Noncontact vibration measurements on compressor rotor blades". *Measurement Science and Technology,* **11**(7), pp. 847–856.

[2] Dimitriadis, G., and Carrington, I., 2002. "Blade-tip timing measurement of synchronous vibrations of rotating bladed assemblies". *Mechanical Systems and Signal Processing,* **16**, pp. 599–622.

[3] Beauseroy, P., and Lengellé, R., 2007. "Nonintrusive turbomachine blade vibration measurement system". *Mechanical Systems and Signal Processing,* **21**(4), May, pp. 1717–1738.

[4] Diamond, D.H, Heyns, P.S, and Oberholster, A.J, 2015. "A Comparison Between Three Blade Tip Timing Algorithms for Estimating Synchronous Turbomachine Blade Vibration". *9th WCEAM Research Papers*, pp. 1–12.

[5] Kumar, S., Roy, N., and Ganguli, R., 2007. "Monitoring low cycle fatigue damage in turbine blade using vibration characteristics". *Mechanical Systems and Signal Processing,* **21**(1), Jan, pp. 480–501.

[6] Russhard, P., 2015. "The Rise and Fall of the Rotor Blade Strain Gauge". *Vibration Engineering and Technology of Machinery,* **23**, pp. 27–38.

[7] Heath, S., and Imregun, M., 1996. "An improved single-parameter tip-timing method for turbomachinery blade vibration measurements using optical laser probes". *International Journal of Mechanical Science,* **38**(10), pp. 1047–1058.

[8] Hu, Z., Lin, J., Chen, Z.-S., Yang, Y.-M., and Li, X.-J., 2015. "A non-uniformly under-sampled blade tip-timing signal reconstruction method for blade vibration monitoring.". *Sensors,* **15**(2), Jan, pp. 2419–37.

[9] Russhard, P., 2013. Timing Analysis. US 8 457 909 B2.

[10] Sabbatini, D., Peeters, B., Martens, T., and Janssens, K., 2012. "Data acquisition and processing for tip timing and operational modal analysis of turbomachinery blades". In 10th International Conference on Vibration Measurements by Laser and Noncontact Techniques, Vol. 60, pp. 52–60.

[11] Chen, Z., Yang, Y., Xie, Y., Guo, B., and Hu, Z., 2013. "Non-contact crack detection of high-speed blades based on principal component analysis and Euclidian angles using optical-fiber sensors". *Sensors and Actuators A: Physical,* **201**, Oct, pp. 66–72.

[12] Russhard, P., 2010. Timing analysis. EP 2 199 764 A2.

[13] Przysowa, R., 2014. "Analysis of synchronous blade vibration with the use of linear sine fitting". *Journal of KONBiN,* **2**(30), p. 17.

[14] Guo, H., Duan, F., and Zhang, J., 2016. "Blade resonance parameter identification based on tip-timing method without the once-per revolution sensor". *Mechanical Systems and Signal Processing,* **66**, Jan, pp. 625–639.

[15] Ivey, P., Grant, K., and Lawson, C., 2002. "Tip timing techniques for turbomachinery HCF condition monitoring". In the 16th Symposium on Measuring Techniques in Transonic and Supersonic Flow in Cascades and Turbomachines, Sept, pp. 1–7.

[16] Joung, K., Kang, S., Paeng, K., Park, N., Choi, H., You, Y., and von Flotow, A., 2006. "Analysis of Vibration of the Turbine Blades using Non-Intrusive Stress Measurement System". In Proceedings of the ASME Power Conference, ASME, pp. 391–397.

[17] Carrington, I. B., Wright, J. R., Cooper, J. E., and Dimitriadis, G., 2001. "A comparison of blade tip timing data analysis methods". *Proceedings of the Institution of Mechanical Engineers, Part G: Journal of Aerospace Engineering,* **215**(5), Jan, pp. 301–312.

[18] Grant, K., 2004. "Experimental Testing of Tip-Timing Methods used for Blade Vibration Measurement in the Aero-Engine". PhD Thesis, Cranfield University.

[19] Gallego-Garrido, J., Dimitriadis, G., Carrington, I. B., and Wright, J. R., 2007. "A Class of Methods for the Analysis of Blade Tip Timing Data from Bladed Assemblies Undergoing Simultaneous Resonances–Part II: Experimental Validation". *International Journal of Rotating Machinery,* **2007**, pp. 1–10.

[20] Gallego-Garrido, J., Dimitriadis, G., and Wright, J. R., 2007. "A Class of Methods for the Analysis of Blade Tip Timing Data from Bladed Assemblies Undergoing Simultaneous Resonances–Part I: Theoretical Development". *International Journal of Rotating Machinery,* **2007**, pp. 1–11.

[21] Mansisidor, M. R., 2002. "Resonant blade response in turbine rotor spin tests using a laser-light probe non-intrusive measurement system". MSc(Aeronautical), Naval Postgraduate School, Monterey, California, Mar.

[22] Jousselin, O., 2013. Blade Tip Timing Uncertainty. EP 26 316 17 A2.

[23] Petrov, E., Di Mare, L., Hennings, H., and Elliott, R., 2010. "Forced Response of Mistuned Bladed Disks in Gas Flow: A Comparative Study of Predictions and Full-Scale Experimental Results". *Journal of Engineering for Gas Turbines and Power,* **132**(5), p. 052504.

[24] Madhavan, S., Jain, R., Sujatha, C., and Sekhar, A. S., 2013. "Condition monitoring of turbine rotor blade on a gas turbine engine". *International Congress on Sound & Vibration,* **20** (July 2013), pp. 7–11.

[25] Cline, A. K., Moler, C. B., Stewart, G. W., and Wilkinson, J. H., 1979. "An estimate for the condition number of a matrix". *SIAM Journal on Numerical Analysis,* **16**(2), pp. 368–375.

[26] Lee, A., 2013. Particle swarm optimization (PSO) with constraint. http://pythonhosted.org/pyswarm/ [Accessed 2017-09-26].

[27] Szczepanik, R., Rzadkowski, R., and Kwapisz, L., 2010. "Crack Initiation of Rotor Blades in the First Stage of SO-3 Compressor". *Advances in Vibration Engineering,* **9**(4), pp. 3–8.

[28] Woike, M. R., Roeder, J. W., Hughes, C. E., and Bencic, T. J., 2009. "Testing of a microwave blade tip clearance sensor at the NASA Glenn Research Center". In Proceedings of the 47th American Institute of Aeronautics and Astronautics Aerosciences Conference.